ISBN: 978-3-95450-247-9 ISSN: 2673-5490 doi: 10.18429/JACoW-IPAC2024-TUPG19

COLLIMATOR STUDY FOR THE DIAMOND-II STORAGE RING

H. Ghasem*, I.P.S. Martin, H.-C. Chao, Diamond Light Source, Oxfordshire, UK
W. Shields, Royal Holloway, University of London, UK

Abstract

Horizontal and vertical collimators will be installed in the Diamond-II storage ring to protect the ring components against undesired losses and radiation showers. Different loss mechanisms have been studied, including lifetime effects, RF trips, injection losses and kicker misfire. In this paper, we present the latest collimator layout and collimation efficiency. In addition, the risk of damage to the collimator blades has been studied for different materials using BDSIM.

INTRODUCTION

There are many sources of beam loss in storage rings and the lost particles may damage equipment such as permanent magnet dipoles or in-vacuum insertion devices (IDs). The pressure profile may also be affected by electrons hitting the vacuum chamber. Therefore, it is vital to protect machine by collecting the losses. In this paper, we introduce the latest layout of the collimators in the Diamond-II storage ring and present collimator performance for the various loss mechanisms and investigate the potential for damage to the collimator blade.

LAYOUT OF COLLIMATORS

There are six collimators in the Diamond-II storage ring, 3 horizontal and 3 vertical. They are in the mid to standard (MS) straight girder sections, located in the downstream half of the dispersion bumps where the beta and dispersion functions are relatively large. The collimator location is free from any engineering restrictions which makes it practical. The general layout of the collimators in all super periods of the storage ring is shown in Fig. 1. The optical functions along one cell of the Diamond-II ring is displayed in Fig. 2. The collimator location is indicated with a dotted line. The length of the collimator blade is 3.5 cm and the minimum gap of the horizontal and vertical collimators is set to 7 mm and 3 mm respectively.

COLLIMATION PERFORMANCE

The performance of the collimators in the ring has been evaluated for the primary loss mechanisms such as RF switch-off, Touschek effect, elastic and in-elastic gas scattering and injection mis-steer. Alignment and multipole errors have been added for 20 seeds in the calculations.

To cover RF trips and deliberate beam dumps, the collimator's effectiveness for capturing losses due to turning the RF cavity off has been investigated by tracking a bunch of 100K particles within a Gaussian distribution in the ring while the RF is off. Due to synchrotron radiation, the particle energies reduce until they are lost on an aperture after about 250 turns.

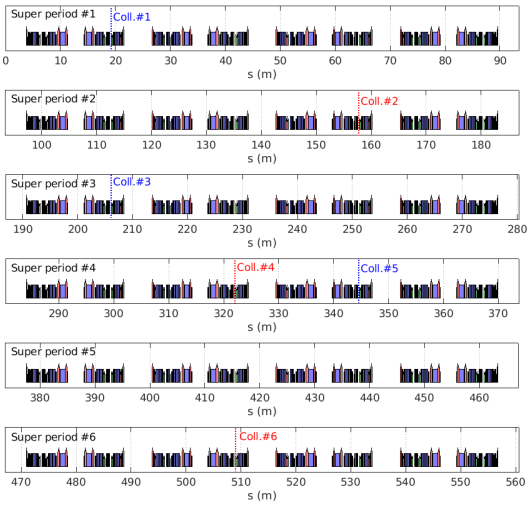

Figure 1: General layout of collimators in Diamond-II ring.

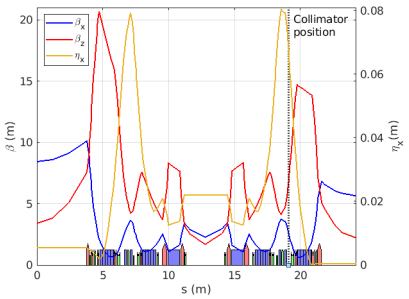

Figure 2: Optical functions along a cell of Diamond-II ring.

To evaluate the performance of the collimators at collecting Touschek losses, many Touschek scatter points have been considered in the lattice and particles tracked through the ring with gradually increased momentum deviation until they get lost on a physical aperture.

Losses due to gas scattering depend on many parameters such as residual gas pressure, momentum aperture and scattering angles. For elastic scattering, an appropriate range scatterning angle has been found using Eq. (1), see Fig. 3.

$$\frac{d\sigma}{d\Omega} = \left(\frac{2Ze^2}{E}\right)^2 \frac{1}{\left(\Theta^2+\Theta^2_{min}\right)^2} \quad (1)$$

In (1), Z is the atomic number, E is energy, e is the electron charge and θ is the scattering angle. The "inelastic_scattering" commands in ELEGANT [2] with an input momentum aperture have been used to compute the distribution of

* hossein.ghasem@diamond.ac.uk

ISBN: 978-3-95450-247-9 ISSN: 2673-5490 doi: 10.18429/JACoW-IPAC2024-TUPG19

inelastic gas scatter losses. Fig. 4 summarises the percentage of losses captured by the collimators for each of these loss mechanisms.

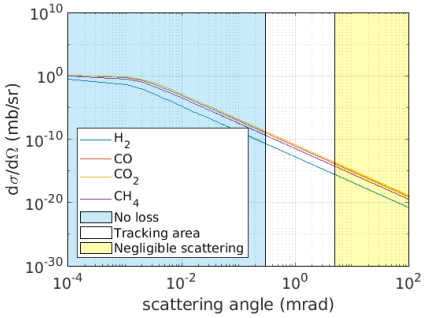

Figure 3: Differential cross section of in-elastic scattering vs scattering angle.

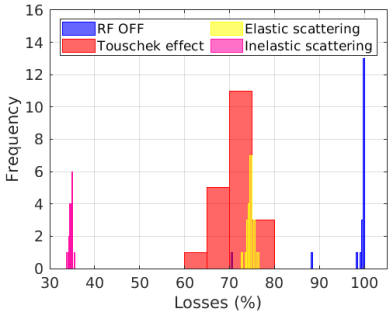

Figure 4: Percentage of losses captured by the collimators for each loss mechanism.

The performance of the collimators for capturing injection losses was assessed by deliberately mis-steering the injected beam for five error seeds to give injection efficiencies around 70%. Table 1 gives a summary of the collimator efficiency. There would be ~14% of the losses due to hor. mis-steers at the septum blade.

Table 1: Mean Percentage of Lost Particles Captured by the Collimators

Loss mechanism	Value (%)
RF switch-off	97.7 ± 6.9
Touschek scatter	71.4 ± 3.4
Elastic gas scatter	74.6 ± 0.8
Inelastic gas scatter	34.7 ± 0.4
Injection, hor. mis-steer	85.5 ± 14
Injection, ver. mis-steer	99.8 ± 0.2

ENERGY DEPOSITION

Collimators are the key components used to protect the machine from lost particles, but they may be damaged by the deposited energy. When a particle hits the collimator, it generates a shower of secondary particles and part of the energy is deposited in the blade. Turning the RF cavity off is planned to be the main method for killing the beam in Diamond-II, and for this, the whole 300 mA beam could be captured by the collimator within a few tens of turns. Fig. 5 shows the distribution of lost particles as well as the amount charge hitting the collimator in each turn for the ideal case with RF off.

It is essential to investigate the potential for collimator damage and the temperature rise caused by the incident particles. For this purpose, the BDSIM [1] code has been used. The energy deposition found from tracking the particle distribution shown in Fig. 5 is displayed in Fig. 6. Different materials have been considered for collimator blade and as shown, a tungsten collimator would have the highest energy deposition due to having the shortest radiation length. The integrated energy deposition along the collimator blade in the transverse plane is shown in Fig. 7 for tungsten. The pixel size is 5 µm x 5 µm.

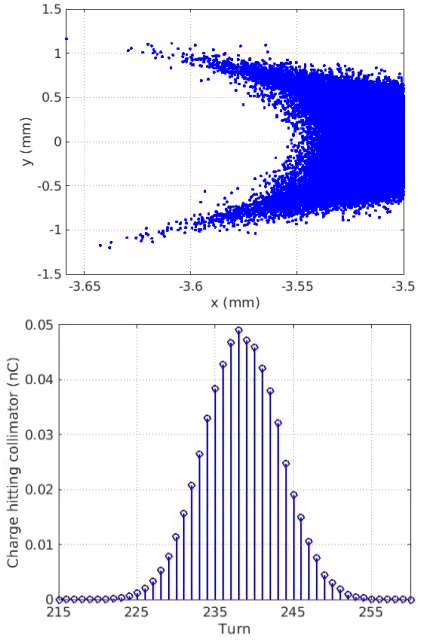

Figure 5: (top) Distribution of losses due to RF OFF and (bottom) amount of charge at collimator.

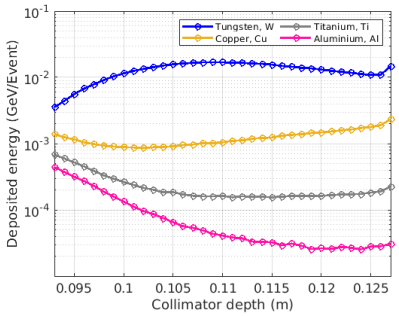

Figure 6: Deposited energy along the collimator length.

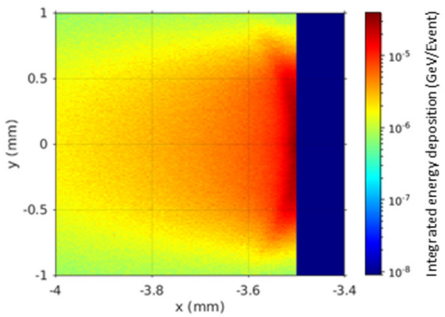

Figure 7: Integrated energy deposition in transverse plane.

ISBN: 978-3-95450-247-9 ISSN: 2673-5490 doi: 10.18429/JACoW-IPAC2024-TUPG19

THERMAL DIFFUSION

As shown in Fig. 5, the majority of the losses are from turn 225 until turn 250 which corresponds to approximately 48.6 µs. Thermal diffusion can diminish the degree of material damage within this time duration by reducing the temperature rise. Thermal diffusion has been approximated by convolving the beam dose map with a Gaussian spread function with standard deviation of thermal diffusivity [3] and creating an effective (total) beam dose map. Using this model, the highest temperature rise occurs at the surface of collimator (slice #1) on turn 242. The integrated energy deposition in the transverse plane including thermal diffusion effect is displayed in Fig. 8 for a tungsten collimator blade.

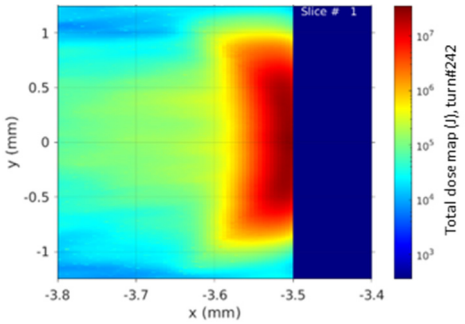

Figure 8: Integrated energy deposition including thermal diffusion in the transverse plane.

The energy deposition in the collimator blade increases its temperature and this can be used to evaluate the volume of material which might be melted. Using Eq. (2), a melting condition is indicated if:

$$\text{Eff. dose} > \rho V C(T_{melt} - T_1) + \Delta H_m \qquad (2)$$

where ρ is the mass density, V is the volume, C is the specific heat capacity, T is the temperature and ΔH_m is the enthalpy of melting. The results shown in Fig. 9 indicate the collimator will melt given the maximum energy deposited in the xy plane, irrespective of the material used.

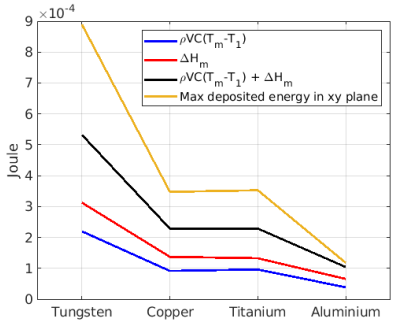

Figure 9: Melting condition for different materials.

FAN-OUT KICKER

To reduce the likelihood of damaging the collimator, a practical solution would be to use fan-out kickers to spread the electron bunches transversely and distribute the energy deposition over a larger area of the blade. For this purpose, one vertical and one horizontal kicker located in straight K24 of the ring with kick angles of 0.2 mrad and 1 mrad respectively have been simulated. Pulse shapes for the horizontal and vertical kicker power supplies are shown in Fig. 10, and the resulting histograms of beam losses in the collimator are shown in Fig. 11. This shows that the energy deposition can be spread over almost 1 mm^2 rather than being concentrated in a single small spot at the level of 100's of microns. Maximum energy deposition in the surface of collimator without and with kickers is 8.72E-6 and 1.36E-6 GeV per event. This work is still in progress.

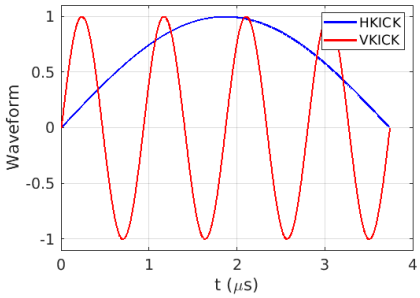

Figure 10: Pulse shape for the fan-out kickers.

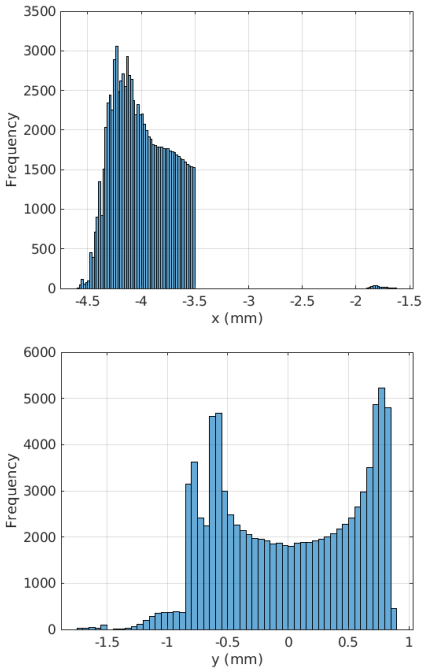

Figure 11: Histogram of losses at the collimators.

SUMMARY AND CONCLUSION

The ability of the collimators to collect losses in the Diamond-II storage ring has been studied, as well as the risk of damage to the blades. The results indicated that the collimators will be melted irrespective of material used. Installing fan-out kickers in one of the empty mid-straights could reduce the collimator damage by spreading the beam over a larger area.

ISBN: 978-3-95450-247-9 ISSN: 2673-5490 doi: 10.18429/JACoW-IPAC2024-TUPG19

REFERENCES

[1] L.J. Nevay, et al., “BDSIM: An accelerator tracking code with particle-matter interactions”, *Com. Phys. Com*. 252, (2020) 107200. doi:10.1016/j.cpc.2020.107200

[2] M. Borland, "Elegant: A flexible SDDS-compliant code for accelerator simulation," Advanced Photon Source LS-287, Sep. 2000. doi:10.2172/761286.

[3] J. Dooling, et al., “Collimator irradiation studies in the Argonne Advanced Photon Source at energy densities expected in next-generation storage ring light sources”, *Phy. Rev. Acc. Beams,* vol. 25, pg. 043001, 2022. doi:10.1103/PhysRevAccelBeams.25.043001